Nuclear Engineering and Technology 51 (2019) 1939–1950

Contents lists available at ScienceDirect

Nuclear Engineering and Technology

journal homepage: www.elsevier.com/locate/net

Original Article

Identification of hydrogen flammability in steam generator compartment of OPR1000 using MELCOR and CFX codes

Joongoo Jeon [a], Yeon Soo Kim [a], Wonjun Choi [a], Sung Joong Kim [a, b, *]

[a] Department of Nuclear Engineering, Hanyang University, 222 Wangsimni-ro, Seongdong-gu, Seoul, 04763, Republic of Korea
[b] Institute of Nano Science & Technology, Hanyang University, 222 Wangsimni-ro, Seongdong-gu, Seoul, 04763, Republic of Korea

ARTICLE INFO

Article history:
Received 8 November 2018
Received in revised form
19 June 2019
Accepted 23 June 2019
Available online 2 July 2019

Keywords:
CFX
MELCOR
Hydrogen
Surge line
Station blackout

ABSTRACT

The MELCOR code useful for a plant-specific hydrogen risk analysis has inevitable limitations in prediction of a turbulent flow of a hydrogen mixture. To investigate the accuracy of the hydrogen risk analysis by the MELCOR code, results for the turbulent gas behavior at pipe rupture accident were compared with CFX results which were verified by the American National Standard Institute (ANSI) model. The postulated accident scenario was selected to be surge line failure induced by station blackout of an Optimized Power Reactor 1000 MWe (OPR1000). When the surge line failure occurred, the flow out of the surgeline was strongly turbulent, from which the MELCOR code predicted that a substantial amount of hydrogen could be released. Nevertheless, the results indicated nonflammable mixtures owing to the high steam concentration released before the failure. On the other hand, the CFX code solving the three-dimensional fluid dynamics by incorporating the turbulence closure model predicted that the flammable area continuously existed at the jet interface even in the rising hydrogen mixtures. In conclusion, this study confirmed that the MELCOR code, which has limitations in turbulence analysis, could underestimate the existence of local combustible gas at pipe rupture accident. This clear comparison between two codes can contribute to establishing a guideline for computational hydrogen risk analysis.

1. Introduction

1.1. Background

The hydrogen combustion in a containment is one of the vulnerable phenomena threatening the safety of a nuclear power plant (NPP) [1]. During a postulated severe accident, a large amount of hydrogen can be generated dominantly through an exothermic reaction of zircaloy and steam. The hydrogen is initially confined in the reactor coolant system (RCS), but can be released into the containment by creep rupture of the hot leg or pressurizer (PRZ) surge line. As hydrogen promptly diffuses throughout the containment atmosphere, highly combustible hydrogen mixtures can be formed. The combustion of these mixtures can impose high pressure and temperature loads to the containment structure depending on the thermodynamic and chemical properties of the mixtures. These loads can damage the containment integrity and, in the worst case, induce containment rupture releasing radionuclides into the ambient environment. Owing to this potential risk of hydrogen combustion, most countries operating and constructing NPPs devote significant attention to prevent such hydrogen risk [2]. In particular, a vigorous computational analysis has been performed on the prototypical scale of the NPP to avert the burden of large experiments on hydrogen combustion.

The PRZ surge line is a pipe connecting the hot leg and PRZ in the RCS. During a severe accident, the temperature and pressure reach more escalating states compared to those of normal operating conditions, and thus, the integrity of the surge line is substantially threatened. When the surge line failure occurred, the flow out of the surgeline was strongly turbulent, from which the MELCOR code predicted that a substantial amount of hydrogen could be released. Previous studies reported that in a pressurized water reactor (PWR), a surge line break could occur by creep rupture. For example, Vierow et al. confirmed that all of the three representative severe accident codes, MELCOR, MAAP4, and SCDAP/RELAP 5, predicted the creep rupture using the Larson–Miller (LM)

* Corresponding author. Department of Nuclear Engineering, Hanyang University, 222 Wangsimni-ro, Seongdong-gu, Seoul, 04763, Republic of Korea
E-mail address: sungjkim@hanyang.ac.kr (S.J. Kim).

https://doi.org/10.1016/j.net.2019.06.024

Abbreviations

ADV	Atmospheric Dump Valve
ANSI	American National Standard Institute
CDV	Condenser Dump Valve
CET	Core Exit Temperature
CFD	Computational Fluid Dynamics
CPR1000	China Pressurized Reactor 1000 MWe
CV	Control Volume
ECCS	Emergency Core Cooling System
IRWST	In-containment Refueling Water Storage Tank
LBB	Leak Before Break
LD	Leakage Detection
LM	Larson–Miller
LOCA	Loss-of-Coolant Accident
LP	Lumped Parameter
MCCI	Molten Corium–Concrete Interaction
MSIV	Main Steam Isolation Valve
MSSV	Main Steam Safety Valve
NPP	Nuclear Power Plant
NSSS	Nuclear Steam Supply System
OPR1000	Optimized Power Reactor 1000 MWe
PRZ	Pressurizer
PSRV	Pressurizer Safety Relief Valve
PWR	Pressurized Water Reactor
RCS	Reactor Coolant System
RPV	Reactor Pressure Vessel
SBO	Station Blackout
SDS	Safety Depressurization System
PHARE	Programme to assist the Central and Eastern European countries

Nomenclature

A	flow-path area (m^2)
A_a	asymptotic area (m^2)
A_e	broken-plane area (m^2)
C_T	thrust coefficient
D	diameter
E	total internal energy (J)
F	open fraction
G_e	mass flux ($kg/m^2 \cdot s$)
g	gravitational acceleration (m/s^2)
$\dot{H}$	nonflow energy source (J/s)
h	specific enthalpy (J/kg)
k	turbulence kinetic energy (m^2/s^2)
L	distance (m)
M	total mass (kg)
$\dot{M}$	nonflow mass source (kg/s)
P_0	stagnation pressure (bar)
P_{LM}	Larson–Miller parameter
p	pressure (Pa)
Pr	Prandtl number
R_i	inner diameter (m)
R_o	outer diameter (m)
R_v	gas constant for water vapor ($J/K \cdot kg$)
T	temperature (K)
T_0	stagnation temperature (bar)
t	time (s)
t_R	time to rupture (s)
U	velocity vector (m/s)

Greek letters

α	volume fraction
θ	jet expansion angle (°)
Γ	volumetric mass source density ($kg/m^3 \cdot s$)
κ	specific heat ratio
λ	thermal conductivity ($W/m \cdot K$)
μ	dynamic viscosity ($Pa \cdot s$)
μ_T	turbulent viscosity ($Pa \cdot s$)
ν	velocity (m/s)
ρ	density (kg/m^3)
σ	direction factor
σ_e	effective stress (Pa)

model. The first failure occurs at the surge line, followed by those of the steam generator (SG) tubes or hot leg piping during a hypothetical station blackout (SBO) scenario [3]. Despite the possibility of surge line failure, no detailed studies on the hydrogen risk have been carried out for this type of failure.

Among the above three severe accident codes, MELCOR is a state-of-the-art severe accident simulation code developed by the Sandia National Laboratories, used to assess plant risks and analyze source terms since 1982. It has been intensively used by regulatory bodies and academic researchers to investigate the potential risks from various severe accident phenomena. It treats the entire spectrum of severe accident phenomena, including RCS and containment thermal-hydraulic responses, core heat-up, fission product transport, and hydrogen behavior in a unified framework [4,5]. Although the MELCOR code is not a combustion-specific code to solve a detailed chemical reaction, identification of the hydrogen behavior is feasible for the combustion risk analysis. Recently, Kim et al. investigated the hydrogen risk for an Optimized Power Reactor 1000 MWe (OPR1000) under an SBO using the MELCOR code [6]. In addition, Choi et al. analyzed the hydrogen mitigation measures of the Canada Deuterium Uranium (CANDU) containment under a loss-of-coolant accident (LOCA) scenario [7]. Kim et al. studied the hydrogen behaviors inside and around an in-containment refueling water storage tank (IRWST) to confirm the integrity of APR1400-IRWST during an SBO accident [8]. In China, Wang et al. analyzed the hydrogen behavior for a China Pressurized Reactor 1000 MWe (CPR1000) under an SBO scenario [9]. To sum up, the MELCOR code has been widely utilized for hydrogen risk analyses of various NPPs for severe accident scenarios.

However, the MELCOR code has some limitations in prediction of turbulent flows of hydrogen mixtures owing to its inherent characteristics of the lumped-parameter (LP) code. As the momentum equation for each flow path is only one-dimensional and there is no momentum associated with control volumes, multidimensional effects associated with advection of momentum cannot be correctly calculated [4]. In addition, it is difficult to obtain the local gas distribution inside the containment by the LP code as each control volume is practically set at the meter-scale. The code provides only the gas concentration of the assigned control volume; it cannot be confirmed whether the gases are locally well mixed. Even if continuous flammable mixtures exist in a part of the control volume, they cannot be identified by the bulk information of the volume. A detailed nodalization method has been introduced by Kim et al. to overcome this limitation, but the trial was not fully successful. They emphasized the necessity of numerous analyses on the fluid behavior by comparing simulation results of the MELCOR code with those of other computational fluid dynamic (CFD) codes [6]. This provided a rationale for this comparison study between

the MELCOR and CFX codes.

The CFX code is a multi-purpose CFD code developed for industrial applications such as fluid and gas dynamics, heat transfer, and chemical combustion. The code solves three-dimensional (3D) fluid dynamic transport equations in a structured multiblock mesh through the finite-volume method. In this study, the continuity, momentum, and energy equations are solved for the analysis of the hydrogen behavior within a specific containment compartment. In addition to the basic solver, the code incorporates turbulence closure models to solve the turbulence effects [10]. Therefore, it is possible to analyze the jet flow of the ultrasonic gas during a pipe rupture. However, simulation of the whole containment is infeasible in the CFD domain owing to its very large volume. In addition, compared to the LP code, it is unrealistic to simulate a complex severe accident scenario implementing a mitigation strategy and occurrence of molten corium–concrete interaction (MCCI). On the other hand, the MELCOR code is fast-running and covers a large scale of control volume size while executing the mitigation strategy. In other word, the both MELCOR and CFD codes have advantages and disadvanges in severe accident analysis. Therefore, a clear comparison between the two codes according to specific accident scenarios, such as pipe rupture, can contribute to establishing a guideline for computational hydrogen risk analysis [11].

Considering the above introduction and motivation, the purposes of this study can be summarized as follows:

1) Analysis of the hydrogen risk in the OPR1000 containment using the MELCOR code during a surge line failure induced by an SBO scenario
2) Analysis of the hydrogen risk in the same accident scenario using the CFX code
3) Comparison between the MELCOR and CFX results to verify the hydrogen risk analysis performed by the MELCOR code under turbulent conditions

Particularly, the prediction accuracy of the local gas distribution in jet flow conditions was analyzed in detail. As it is difficult to simulate the severe accident sequences in the RCS using the CFX code, thermal-hydraulic variables of the MELCOR results were used as initial and boundary conditions. In addition, the CFX results were verified by comparison with the American National Standard Institute (ANSI) model. The MELCOR version 1.8.6 and CFX version 17.0 were utilized in this study.

1.2. Model difference between the MELCOR and CFD codes in the gas behavior analysis

The thermal-hydraulic behavior in MELCOR is governed by the conservation equations of mass, momentum, and energy. They were derived by suitable integrations of the 3D partial differential equations, over a volume for the scalar mass and energy equations, and along a line for the vector momentum equation [12]. Eq. (1) is the differential equation expressing the conservation of mass, where Γ is the volumetric mass source density. In MELCOR, the equation is integrated over a control volume, as expressed by Eq. (2), where M is the total mass [kg], the subscripts i and j refer to the control volume and flow path, respectively, and σ is a factor representing the direction of the flow in the flow path. $\dot{M}$ includes all nonflow sources such as condensation/evaporation, bubble separation, and contributions from other packages such as the BUR and PAR packages in MELCOR. The set of equations cannot be used to simulate a 3D flow; it can solve the flow based on the flow path artificially connected to each control volume. In this case, the local fluid behavior inside the control volume is difficult to identify. The energy conservation equation was derived similarly from the partial differential equations, while neglecting the potential energy and volume-averaged kinetic energy terms, as shown in Eq. (3), where h is the specific enthalpy [J/kg] and $\dot{H}$ is the nonflow energy source [J/kg·s]. The momentum equation also did not consider the kinetic energy terms related to turbulent effects. The only way to simulate the pressure drop due to the turbulent effects is to include the user input directly into the equation. However, the previous experimental or elaborate numerical researches in corresponding flow conditions are required to enter valid values for this user input. It means that the current, MELCOR code cannot predict the local gas behavior even with a very fine nodalization because of this turbulence-unresolved approach.

$$\frac{\partial \rho}{\partial t} + \nabla \cdot (\rho v) = \Gamma \tag{1}$$

$$\frac{\partial M_{i,m}}{\partial t} = \sum_j \sigma_{ij} \alpha_j \rho^d_{j,m} v_j F_j A_j + \dot{M}_{i,m} \tag{2}$$

$$\frac{\partial E_i}{\partial t} = \sum_j \sigma_{ij} \alpha_j \left(\sum_m \rho^d_{j,m} h^d_{j,m} \right) v_j F_j A_j + \dot{H}_i \tag{3}$$

On the other hand, in the CFX code, the set of equations to solve are the Navier–Stokes equations, which explicitly reflect turbulent effects. The main reason why turbulent effects should be considered in the combustion risk is that accurate prediction of gas behavior in the containment is essential for flammability analysis. It is noted that the turbulence is the dominant mechanism in the mixing and dilution of gaseous releases associated with the presence of the structures under atmospheric conditions [13]. Eqs. (4)–(6) are the continuity, momentum, and energy equations, respectively, where μ_T is the turbulent viscosity, k is the turbulence kinetic energy, and Pr_T is the turbulent Prandtl number [10]. Eddy-viscosity turbulence models suggest that the turbulence consists of small eddies continuously forming and dissipating. Among them, the two-equation models including the k–ε standard, k–ω standard, and shear stress transport (SST) models, assumed that the Reynolds stresses are linearly proportional to the mean velocity gradient. It should be noted that the inherent modeling of stress anisotropies theoretically makes the Reynolds stress model more suited for complex flows, but often not better than the two-equation models [14]. The SST model employed in this study uses a k–ω formulation in the inner parts of the boundary layer. Therefore, the SST k–ω model can be used as a low-Re turbulence model without any extra damping functions. The model also switches to a k–ε behavior in the free-stream and thereby avoids the common k–ω problem that the model is too sensitive to the inlet free-stream turbulence properties [15]. Another difference in the CFX code is the prediction capability of the local gas distribution. The CFX code which is based on a very fine mesh, then there is no need to set an artificial flow direction σ like in MELCOR code. Therefore, the fluid moves realistically according to the predicted three-dimensional pressure potential and the equation includes the velocity vector $\vec{U}$.

$$\frac{\partial \rho}{\partial t} + \nabla \cdot (\rho \vec{U}) = 0 \tag{4}$$

$$\frac{\partial \rho U}{\partial t} + \nabla \cdot (\rho \vec{U} \otimes \vec{U}) = (\rho - \rho_0) \vec{g} + \nabla \cdot (\mu + \mu_T) \left((\nabla \cdot \vec{U}) + (\nabla \cdot \vec{U})^T \right) + \nabla \cdot \left(p + \frac{2}{3} \rho k \right) \tag{5}$$

$$\frac{\partial \rho H}{\partial t} + \nabla \cdot (\rho \vec{U} H) - \nabla \cdot \left(\lambda \nabla T + \frac{\mu_T}{Pr_{T,H}} \nabla i \right) = \frac{\partial P}{\partial t} \quad (6)$$

2. MELCOR simulation

2.1. MELCOR input model of OPR1000

The OPR1000 was selected as a reference NPP. It consists of two loops of nuclear steam supply system (NSSS). The original MELCOR base input model simulates the fluid behaviors inside the RCS with dozens of control volumes, as shown in Fig. 1. The RPV comprised a core (CV 170), downcomer (CV 130), lower plenum (CV 150), and upper plenum (CV 260). Four cold legs (CV 380, 390, 480, 490) and two hot legs (CV 310, 410) are connected between the RPV and SG (CV 330, 337, 600, 610, 430, 437, 700, 710). Two safety depressurization system (SDS) valves and pressurizer safety relief valve (PSRV) are connected with a PRZ (CV 500). Opening and closing set points of the PSRV are RCS pressures of 17.24 and 14.1 MPa, respectively. When the RCS pressure decreases to 4.3 MPa, safety injection tanks (CV 382, 392, 482, 492) are passively actuated. On the other hand, SGs are equipped with main steam isolation valves (MSIVs), main steam safety valves (MSSVs), eight condenser dump valves (CDVs), and four atmospheric dump valves (ADVs) [6,7].

A detailed modeling of the containment is essential for an accurate hydrogen risk analysis using the MELCOR code, as hydrogen combustion can occur in the compartments with high hydrogen concentrations associated with complex geometrical characteristics of the containment structures and fluid transportation paths. Therefore, a more detailed nodalization of the containment into 20 compartments was performed by Kim et al. [6]. The SG compartment with the surge line was also included in the nodalization. In order to justify the compatibility of the modeling, the nodalization was performed based on the compartment configuration of the MAAP-CONTAIN analysis, which was submitted to cope with the hydrogen risk regulation. Moreover, all of the nodalization data were obtained from the final safety analysis report (FSAR) on the containment layout of the Shin Kori NPP Units 1 and 2, which are up-to-date OPR1000 [16].

Investigations of the surge line rupture and corresponding hydrogen risk are the main objectives of this study. The surge line was modeled by a control volume connecting the PRZ (CV 500) and hot leg (CV 310), as shown in Fig. 1. The inner and outer diameters of the surge line obtained from the FSAR are 0.3048 and 0.3714 m,

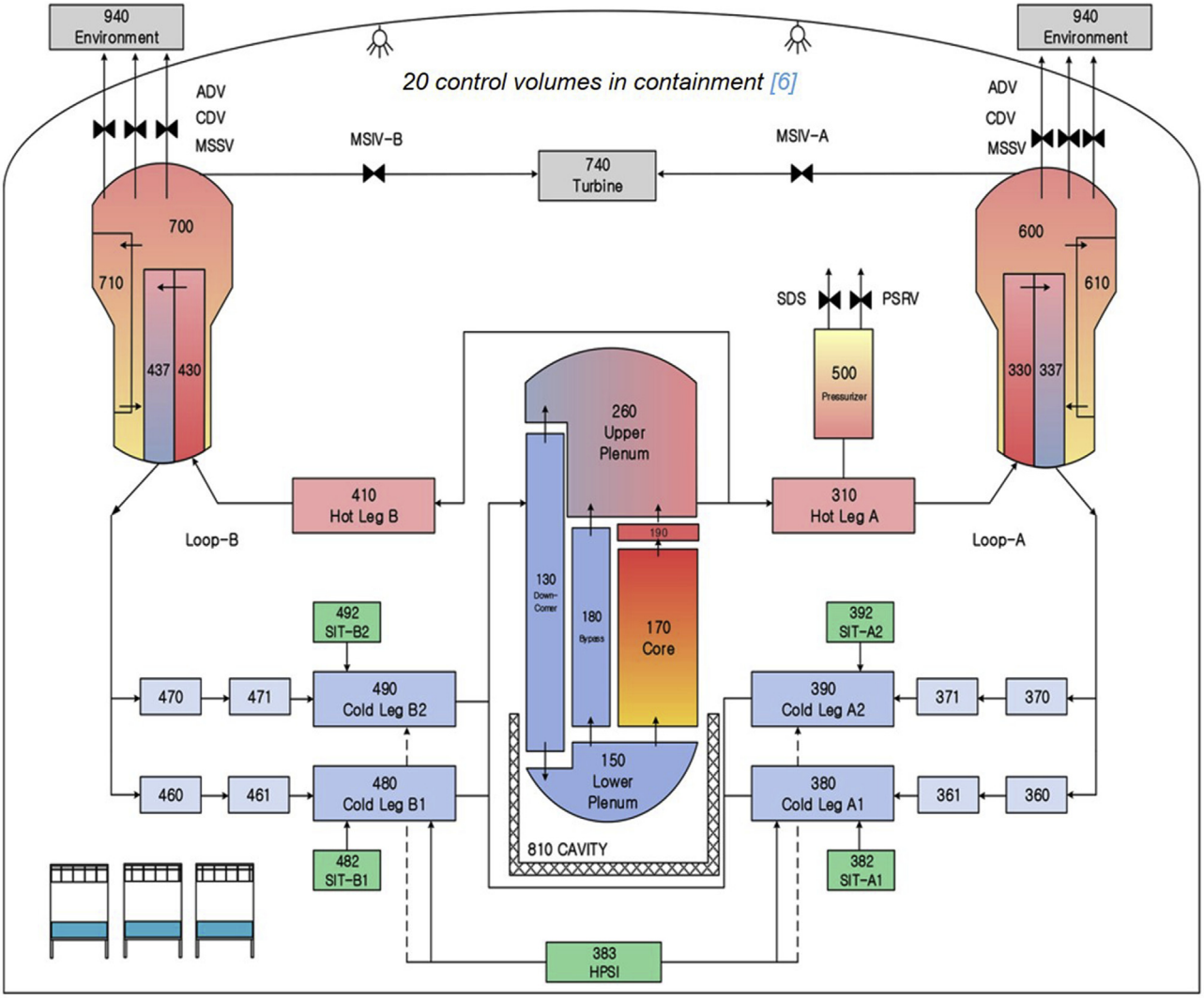

Fig. 1. MELCOR nodalization for OPR1000.

respectively. In order to simulate the pipe rupture, a legitimate rupture model should be included in the MELCOR input. In this study, the LM model in the MELCOR code was selected to predict the creep rupture of the surge line. The model calculates the time to rupture t_R by the average wall temperature T and LM parameter P_{LM} in Eq. (7). The constant C_2 is determined by the material properties; stainless steel was used for the surge line. The parameter is calculated as a function of the effective stress σ_e with constants C_2 and C_3 related to the material properties, as shown in Eq. (8). The effective stress can be calculated by Eq. (9), assisted by the data of geometrical parameters and pressure difference ΔP. As the stress and temperature are not constant, a fractional lifetime rule is applied, and the rupture is assumed to occur when LM-CREEP in Eq. (10) reached the value of 1.0 [4]. Upon the surge line rupture, a large amount of gas mixtures containing hydrogen is released into the SG compartment. As the LM model in MELCOR cannot be used to calculate the rupture area, the rupture area was assumed to be 0.258 cm^2, which was used to analyze the leak before break (LBB) at the primary coolant loop in the FSAR. The leakage detection (LD) system installed in OPR1000 should be able to detect a leakage corresponding to 1/10 of the area within 1 h. If the flammability of the compartment is predicted by the gas release with the LBB, it is difficult to guarantee the consideration on the hydrogen risk in the SG compartment when the operator carries out the mitigation strategies. This implies that the analysis with the LBB enables to investigate the more realistic hydrogen risk induced by the surge line failure. This is consistent with the main objective in this study to compare the MELCOR and CFX codes for prediction of the hydrogen risk under turbulent flow conditions.

$$t_R = 10^{(P_{LM}/T - C_1)} \tag{7}$$

$$P_{LM} = C_2 + C_3 \log_{10}\sigma_e \tag{8}$$

$$\sigma_e = \frac{\Delta P}{R_o^2 - R_i^2} R_i^2 \tag{9}$$

$$LM - \mathrm{CREEP}(t) = \int \frac{\mathrm{d}t}{t_R(t)} \sim \sum \frac{\Delta t_i}{t_R(t_i)} \tag{10}$$

A steady-state calculation was carried out using the input model of OPR1000 to verify its reliability by comparing with the nominal values in the FSAR [16]. Table 1 compares the steady-state parameters of the OPR1000 in the FSAR and MELCOR simulation. The MELCOR results are in good agreement with the FSAR values and thus the reliability of the MELCOR input model could be confirmed.

2.2. MELCOR results related to a primary system analysis

After the verification of the steady-state of the MELCOR input model, SBO accident sequences were simulated. An SBO accident initiated by loss of an off-site power signal was assumed, and the off-site power and secondary feed water were stopped since that moment. For a conservative approach, emergency core cooling system (ECCS) and secondary side cooling were assumed unavailable. The overall sequences of the SBO accident obtained by the MELCOR simulation are shown in Table 2. Although the reactor trip occurred as soon as the accident initiated, the coolant temperature in the reactor started to increase by the decay heat. Fig. 2 shows the behavior of the core exit temperature (CET). The CET is a deterministic parameter used to diagnose the in-vessel coolability of the reactor core during a severe accident [17]. The temperature gradually increased until approximately 2 h only by the decay heat. Since then, the temperature rapidly increased owing to the oxidation heat generated by the exothermic chemical reaction of the hot steam and fuel cladding. As the SG was already dried out, it was not possible to cool the RCS without the mitigation strategies. Fig. 3 shows the behavior of the core water level based on the core control volume (CV 170). Owing to the repetitive discharge through the PSRV, the RCS coolant was depleted and finally the core dry out occurred at 2.62 h. Therefore, the reactor core was degraded due to the insufficient core cooling and the molten core was relocated to the lower plenum. During these series of accident sequences, the temperature of the heat structures constituting the RCS continued to increase. The temperature gradually increased at the beginning of the accident. However, it started to rapidly increase after the RCS coolant was dried out. Eventually, the surge line was ruptured at 3.16 h when the averaged surge line wall temperature was approximately 1200 K. It should be noted that Vierow's MELCOR simulation also predicted the surge line failure at a similar wall temperature. This consistency is reasonable as the LM model predicts pipe rupture based on the wall temperature and pressure difference between the inside and outside of the pipe. Finally, the RPV failure occurred at 4.38 h as the enthalpy release through the assumed rupture area is quite small, compared to the residual heat in the reactor core.

Table 3 shows major parameters of the discharged gas mixture immediately after the rupture. The primary system loosing coolability exhibited a higher pressure than that under the normal operation condition due to the extreme evaporation of the coolant. As an abundant steam was already released by the PSRV, the SG compartment also exhibited a higher pressure than atmospheric pressure. The increased steam fraction of the compartment can be attributed to the same factor. As the surege line ruptured, a large amount of mixture was released into the compartment due to the large pressure difference. The temperature of the released gas mixture is approximately 1400 K, which is higher than the surge line wall temperature. The hydrogen mass fraction of the gas mixture is 0.08, which exceeds 40% in terms of volume fraction. As the flammability of the gas mixture was mainly determined by the volume fraction, this concentration emphasizes the need for a flammability analysis of the SG compartment. It is worth noting that the above MELCOR results were also utilized as the initial and boundary conditions for the CFX simulation.

Table 1
Comparison of the OPR1000 operating conditions of OPR1000 and MELCOR simulation.

Parameter	OPR1000	MELCOR
Core thermal power (MWt)	2815	2815
RCS pressure (MPa)	15.5	15.5
Core inlet temperature (K)	569	573
Core outlet temperature (K)	600	603
Primary flow rate (kg/s)	15306	15546
Secondary side pressure (MPa)	7.37	7.37
Steam flow rate per SG (kg/s)	800	809

Table 2
SBO accident sequences obtained by MELCOR.

Event	Time (h)
Accident start	0
Reactor and RCP trip	0
Oxidation start	2.27
Core dry out	2.61
Cladding melting	2.65
UO_2 melting	2.69
Relocation to the lower plenum	2.72
Surge line failure	3.16
RPV failure	4.38

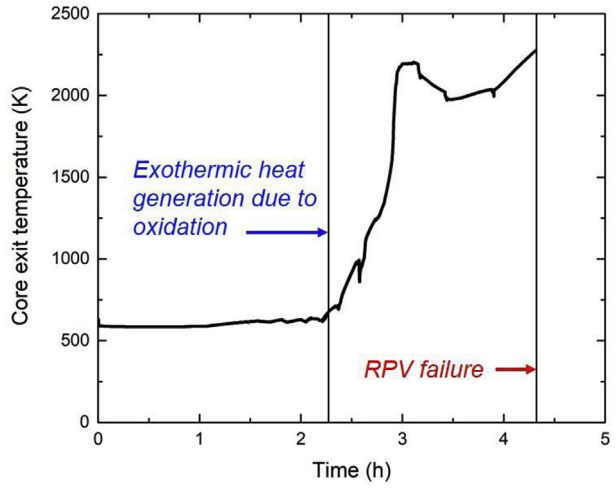

Fig. 2. Behavior of the CET during the SBO scenario.

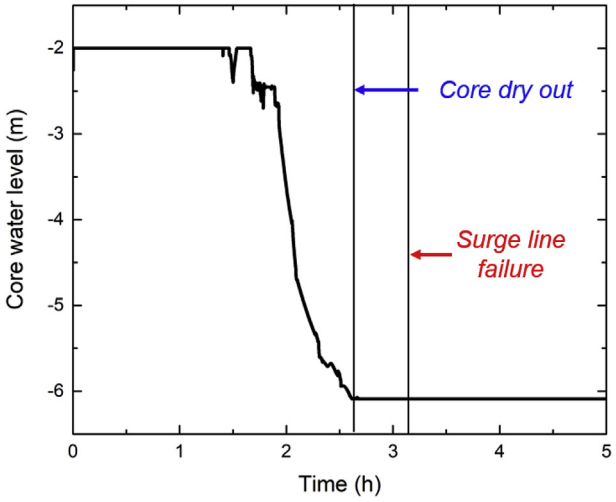

Fig. 3. Behavior of the core water level during the SBO scenario.

Table 3
Major parameters of the emitted gas mixture.

Parameter	Value
Surge line break time (h)	3.16
Surge line	
Pressure (MPa)	17.1
Temperature (K)	1425
Gas mixture composition	(0.08/0.92/0)[a]
SG compartment	
Pressure (MPa)	0.16
Temperature (K)	350
Gas mixture composition	(0/0.17/0.83)[a]

[a] Mass fractions of hydrogen/steam/air.

3. CFX simulation

3.1. Modeling

Unlike the MELCOR simulation, the CFX simulation could be used to analyze the hydrogen behavior in a 3D geometry. Fig. 4 shows the 3D geometry of the SG compartment used to simulate the release of gas at the surge line rupture. The geometry is composed of the surge line, hot leg, and SG, as in the MELCOR code. The shape of each structure was assigned in accordance with the FSAR for Shin Kori 1 and 2 [16]. The simulation domain for observing the hydrogen mixture behavior is the free volume considering the surrounding structures. The rupture area was assumed to be simple geometry based on LBB analysis as with the MELCOR analysis because the MELCOR code cannot predict the rupture area or shape. Although this circular inlet may not reflect actual rupture shape, it cannot have a noticeable effect on the flammability analysis caused by mixing with the atmosphere. The simulation was carried out under the transient condition.

Based on this geometry, a meshing suitable for the CFX analysis was performed. As a first step, we identified that the mesh was structured in the simulation domain as shown Fig. 5. The enlarged mesh structure shows the uniform rectangular mesh in the front and SG adjacent gas elevation zones. The gas released from the inlet was expanded in the free volume and then rose through the hot leg surface. In expansion region with the fastest velocity, the mesh size for close to a unit Courant number is recommended. Since the maximum velocity calculated by the preliminary analysis was close to 1000 m/s, the mesh size near the inlet was determined to be 1e-3 m and the timestep 1e-6 s. To reduce the computing load, the mesh size was set to increase gradually as the distance from the inlet increases, based on the unit Courant number. When the released gas passed through near the hot leg surface, the flow was divided into viscous wall layer, overlap layer and outer turbulent layer. Because the flow beyond the overlap region is main interest in our study, we can use wall function approach in turbulence closure model which relatively less burden on mesh size. The SST turbulence model was chosen as the turbulence closure model. In this case, the general constraint of the mesh size near the wall is extended to a non-dimensional wall distance y^+ of 300 [15]. The maximum y^+ of the mesh near the wall, in this study, was about 160 which is included in this constraint.

In the CFD analysis, the quality of the gridded mesh should be confirmed, as the mesh generation is an important step determining the accuracy and convergence of the analysis. The mesh constructed in this study had a maximum skewness of 0.65 and minimum orthogonality of 0.51 which were considered to be stable values recommended by the ANSYS user's guide. It had a maximum aspect ratio of 11, which was also recommended below 18–20 in the ANSYS document [15]. The number of appropriate mesh nodes to ensure stabilities of all the above conditions was determined to be approximately 4 million. After completion of the meshing, the CFX analysis was performed with the initial and boundary conditions shown in Table 3.

Because it is difficult to reflect all the severe accident sequences occurring in the primary system into the CFX code, thermal-hydraulic variables extracted at the time of the rupture through the MELCOR results were used. Similar coupled analyses of the LP and CFD codes have been used in previous studies to mitigate the inherent limitation of each code [18–20]. The inlet was set to a pressure inlet condition of 17.1 MPa, and temperature and composition ratio were the same as in Table 3. The top and bottom surfaces were set to opening condition as containment atmosphere. This opening boundary condition allows the fluid to cross the boundary surface in either direction. If flow is directed out of the domain, then the condition becomes identical to the pressure outlet boundary (0.16 MPa). In addition, the simulation assumed that the effect of condensation was not discernible as the ambient temperature of the SG compartment is already high, close to 80 °C in the considered time domain. Although we performed CFX modeling considering key factors thoroughly including non-dimensional wall distance and Courant number, it is essential to validate the reliability of mesh and timestep by benchmarking study.

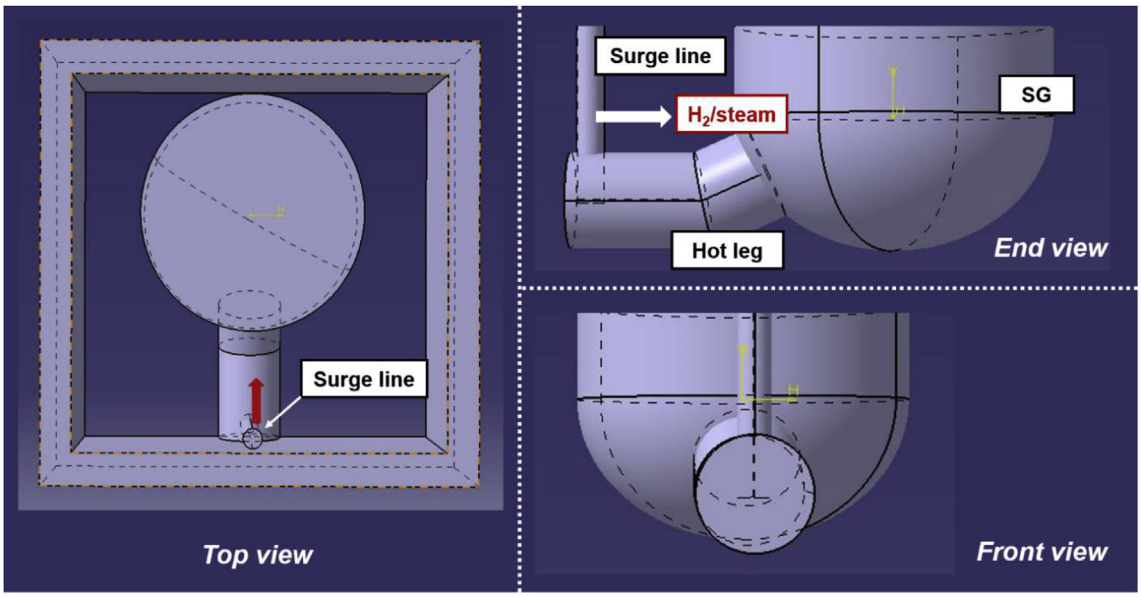

Fig. 4. SG compartment geometry for the CFX simulation.

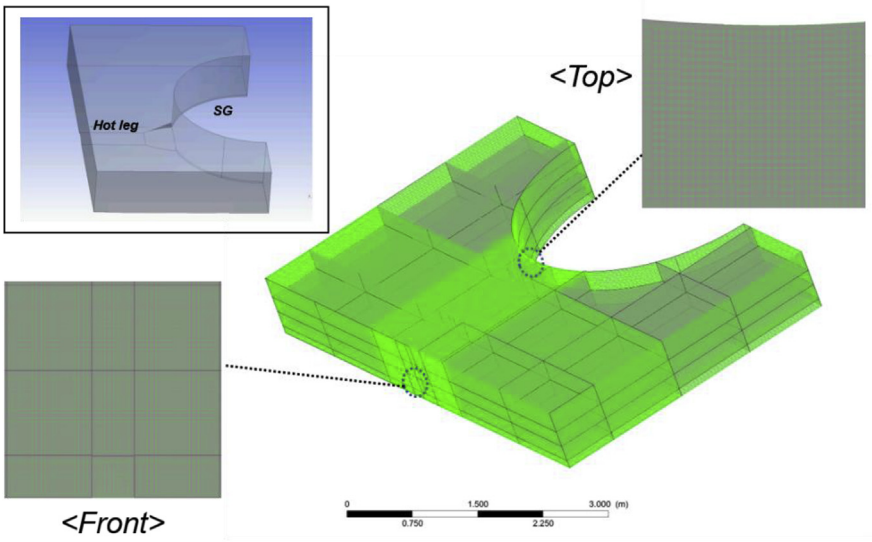

Fig. 5. Structured mesh of SG compartment for CFX simulation. The enlarged mesh structure is for the front and gas elevation zone respectively.

3.2. Validation of the CFX results for the jet shape

Prior to the detailed hydrogen risk analysis using the CFX results, the simulation results were compared with those of the reference pipe rupture model. The ANSI developed a model for prediction of steam emissions with experimental observation when a pipe is involved in RCS breaks. Fig. 6 shows a schematic of a jet divided into three sections, used in the ANSI standard model. Region 1 is the section behind the pressure boundary when the jet exits. In this region, the gas does not contact the gas in the outer region. Region 2 is the section where the jet is under free expansion and thereby an ultrasonic jet is formed. The jet expansion angle θ is influenced by the shock wave pattern and expansion of the fluid. Region 3 is the section where the gas expands in the atmosphere as the jet speed decreases. The major parameters determining the properties of the jet are the mass flux of the emitted gas and jet expansion angle. These parameters were evaluated through the ANSI standard according to the following equations. Eq. (11), included in the model, predicts the mass flux G_e per unit time by variables such as pressure and temperature at the stagnation point. P_0 is the stagnation pressure, T_0 is the stagnation temperature, and R is the ideal gas constant. The ratio of the asymptotic plane area A_a to the broken plane area A_e is evaluated by Eq. (12) using the mass flux, where C_T is the thrust coefficient. Finally, the jet expansion angle can be calculated by Eq. (13) using the length from the break plane to the asymptotic plane L_a [21].

$$G_e = \left[\frac{\kappa}{R_v}\left(\frac{2}{\kappa+1}\right)^{\frac{\kappa+1}{\kappa-1}}\right]^{\frac{1}{2}} \frac{P_0}{T_0^{1/2}} \tag{11}$$

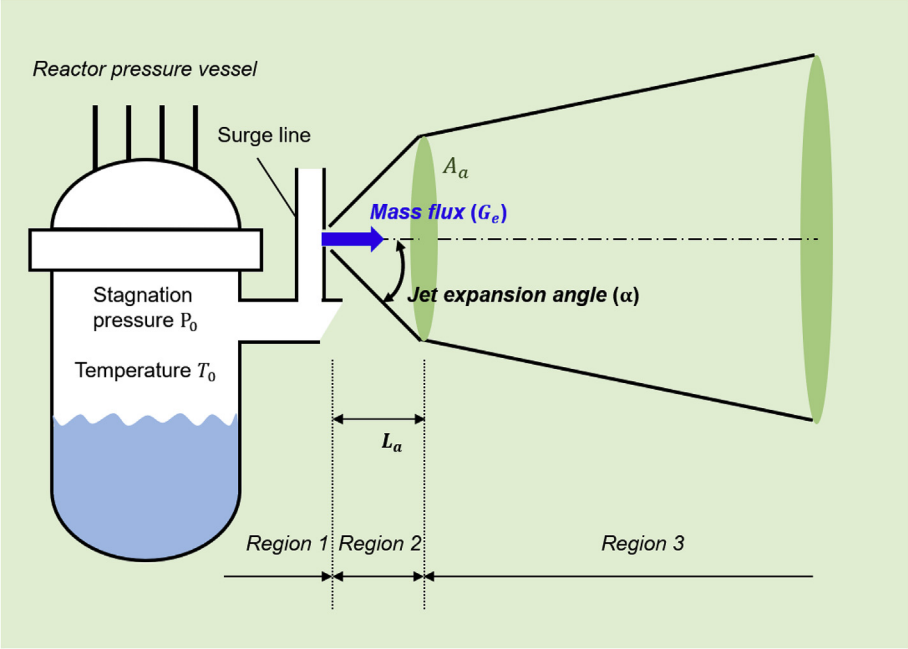

Fig. 6. Jet shape in the ANSI standard model (surge line failure).

$$\frac{A_a}{A_e} = \frac{G_e^2}{\rho_a C_T P_0},\ C_T = 1.26 - \frac{P_{amb}}{P_0} \tag{12}$$

$$\frac{L_a}{D_e} = \frac{1}{2\tan\theta}\left(\sqrt{\frac{A_a}{A_e}} - 1\right) \tag{13}$$

Table 4 compares the CFX simulation results with the evaluated values of the ANSI model. With the ANSI model, the expansion angle was calculated based on the distance L_a of the CFX results. The simulation for the verification sets the release gas only with steam as in the ANSI model. The mass flux per unit time was almost the same. The jet expansion angle in the CFX results was 42°, as shown in Fig. 7, which led to a relative error of approximately 19% with respect to the ANSI model. The error in the angle is increased owing to the simultaneous effects of the errors in the mass flux and distance L_a. A sensitivity analysis of mesh size and timestep can elucidate the cause of this error, but these results suggested that a reasonable gas behavior analysis in a jet simulation can be possible through the current CFX modeling.

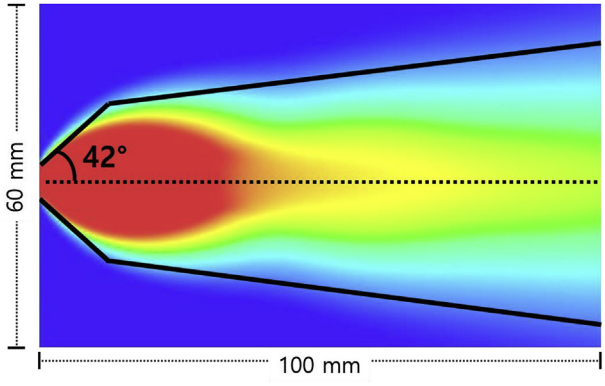

Fig. 7. Jet expansion angle obtained by the CFX results.

4. Results and discussion

4.1. MELCOR simulation results

Fig. 8 shows the volume concentrations of hydrogen and steam in the SG compartment. When the PSRV started to open, the steam concentration rapidly increased, over 20%. At this time, hydrogen was not released into the compartment as the oxidation had not yet occurred in the reactor core. However, oxidation heat was generated with the progress of the accident and the hydrogen gas was released to the containment. The hydrogen concentration of the SG compartment intensively increased after the surge line rupture at 3.16 h. This implies that the flammability needs to be determined under this circumstance of the gas and steam mixtures for a reliable hydrogen risk analysis of the containment. Considering that the flammability depends on numerous factors including the direction of flame propagation, mixture temperature, and presence of diluents such as nonflammable gases, it cannot be reasonably determined only by the concentration of a single gas, as routinely implemented in the MELCOR default model. The default model cannot consider the variation in the flammability limit of hydrogen dependent on the steam concentration.

Regarding the flammability determination, Kumar measured the flammability limits for various hydrogen–air–steam mixtures near 100 °C based on the volume fraction of each gas constituent. The Kumar's flammability limit was analyzed and mapped (Fig. 9), which was then used for flammability determination in this study [22]. Although studies for theoretical flammability limit models have been actively conducted recently [23], the hydrogen mixture

Table 4
Comparison of the ANSI model results with the CFX results.

Parameter	ANSI	CFX	Relative error
Mass flux (kg/m^{2}s)	13969	14394	3%
Jet expansion angle (°)	52	42	19%

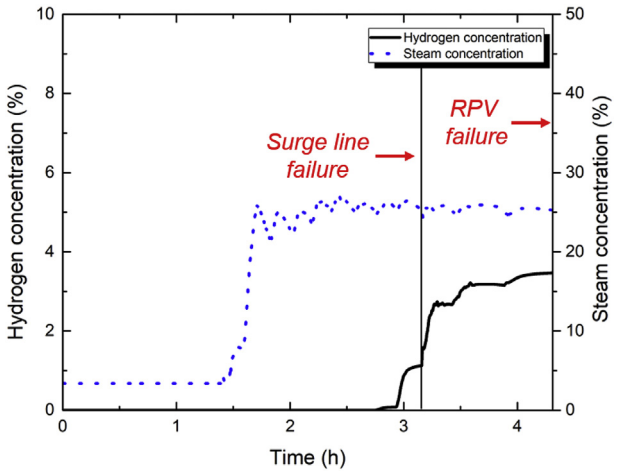

Fig. 8. Volume concentrations of the gas mixtures in the SG compartment under the SBO scenario.

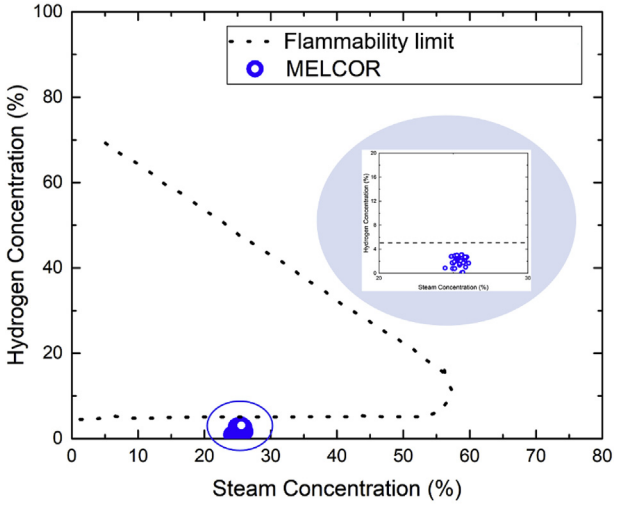

Fig. 9. Absence of flammable mixtures in the SG compartment until RPV failure.

conditions in our CFX simulation almost concur with the Kumar's experiments. The MELCOR results were analyzed based on the time until RPV failure and added to the Kumar's flammability map; no possible flammable region was identified for all of the simulated periods. The hydrogen concentration from the MELCOR results did not exceed the lower flammability limit, as a high concentration of steam was already present in the compartment at the time of hydrogen release. In other words, the released gas did not lead to a sizable effect on the average gas concentration of the compartment. However, in a real situation, the released gas with high pressure difference forms jet shape and extrudes the existing gas. In the peripheral jet region, local combustible mixtures are likely to be present considering the smaller influence of the existing gas. However, it is impossible to simulate these local phenomena at the jet formation using an LP code such as the current MELCOR code.

4.2. Detailed CFX simulation results

Fig. 10 shows a local contour of the hydrogen–steam mixture released upon the surge line rupture, assuming the rupture occurred at the time moment 0 s. At the beginning of the discharge, local vortices were formed; after 10 ms, they transitioned in the form of a well-developed jet without vortex. Subsequently, the process entered the steady-state region beyond the transient state. Fig. 11 shows a global contour of the SG compartment based on the hydrogen mass fraction since 10 ms. The discharged gas mixture was dispersed across the compartment at speed over 1000 m/s and hit the SG. After it encountered the SG, the ascending flow was predicted to dominate the overall domain. The ascending gas mixture can be connected into the gas in the containment dome if the rising mixture does not meet the blockage. This implies that, by an unpredictable ignition, the flammable rising gas mixture can lead to flame propagation across the containment. Aldemir et al. investigated the ignition probability as a function of time immediately after a creep rupture of the surge line following the SBO scenario in a PWR. The ignition can occur at various hydrogen concentrations with different probabilities, based on the discretization of the hydrogen concentration/ignition probability curve [24]. Consequently, the flammable gas mixture induced by the surge line rupture can increase the combustion risk for containment.

Based on these CFX results, the flammability of the mixtures was analyzed in further detail, compared to the case with the MELCOR results. In order to more accurately predict the amount of continuous flammable mixture, combustion phenomena as well as distribution should be numerically simulated. However, the simulation of combustion in a large domain such as containment building consumes enormous computing costs. Therefore, many studies including the Programme to assist the Central and Eastern European countries (PHARE) project have been used concept of flammable cloud to analyze the combustion risk. They calculated the gas distribution in the containment using the CFD-level code, then predicted a flammable cloud by connecting the flammable volume based on the fine mesh. The total volume of flammable cloud was considered to be the amount of flammable mixtures when ignition occur [25]. The flow condition tends to enhance the combustion rate and thus can expand the flammable region [26]. However, since the exact effects of the turbulent condition on flammability limit have not been fully understood, the flammability of each mesh was predicted based on a criterion for mixtures of quiescent state. It is noted that Kim et al. computationally identified that the flammable cloud approach is reasonable method by a result of flame front simulation using the OpenFOAM combustion solver [27]. Therefore, we also predicted the existence of flammable mixture based on the flammability of each mesh.

The mixture hydrogen concentration at the centerline of the rupture position was very high (up to 43%), but the concentration of air was insufficient to generate the combustion as shown Fig. 11. Therefore, they did not belong to the flammable region. As the released gas mixture was dispersed in the radial direction into the SG compartment, the hydrogen concentration was relatively low, but the oxygen concentration increased. Consequently, both hydrogen and oxygen concentrations outside the formed jet belonged to the combustible region. In other words, from the interface between the jet and ambient, the mixture started to have flammable properties regardless of the distance from the rupture position. We displayed the simplified flammable area according to the distance from the rupture position in Fig. 12. For all hydrogen mixtures in the classified flammable area, the flammability was predicted as shown in Fig. 5. Because the data along the distance was easily overlapped in Kumar's flammability map, only some of the data were represented. The inner diameter of the area gradually decreased as gas dispersed, but the outer diameter remained almost constant. This almost constant flammable area suggests that the jet flow can generate continuous flames by ignition. In the ascending flow, which was rapidly diffused into the compartment as it hit the SG, the hydrogen concentration was relatively lower

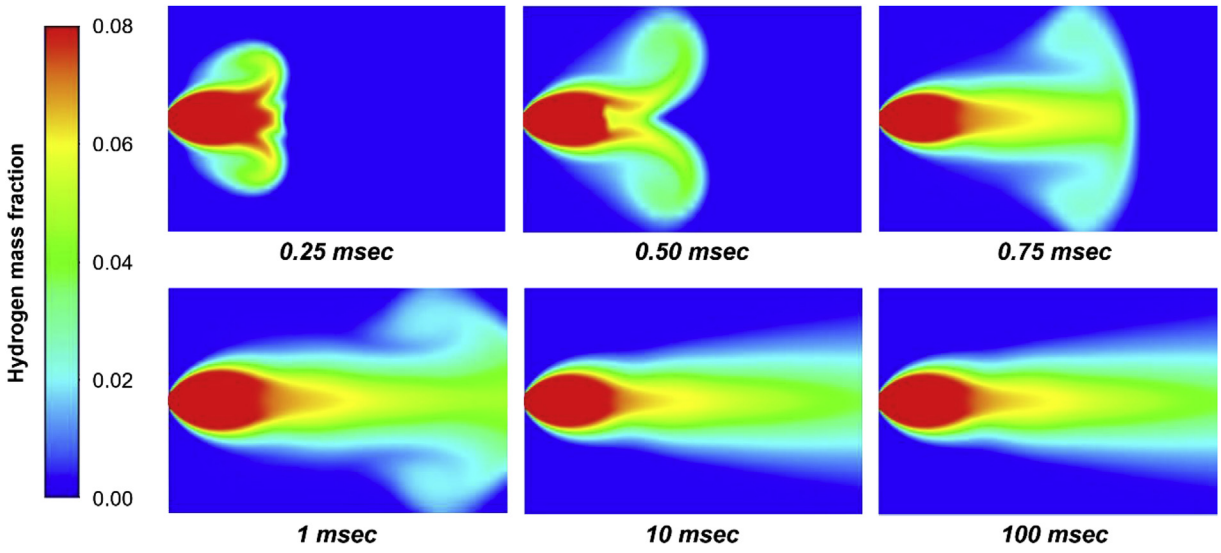

Fig. 10. CFX local contours of the released gas mixture.

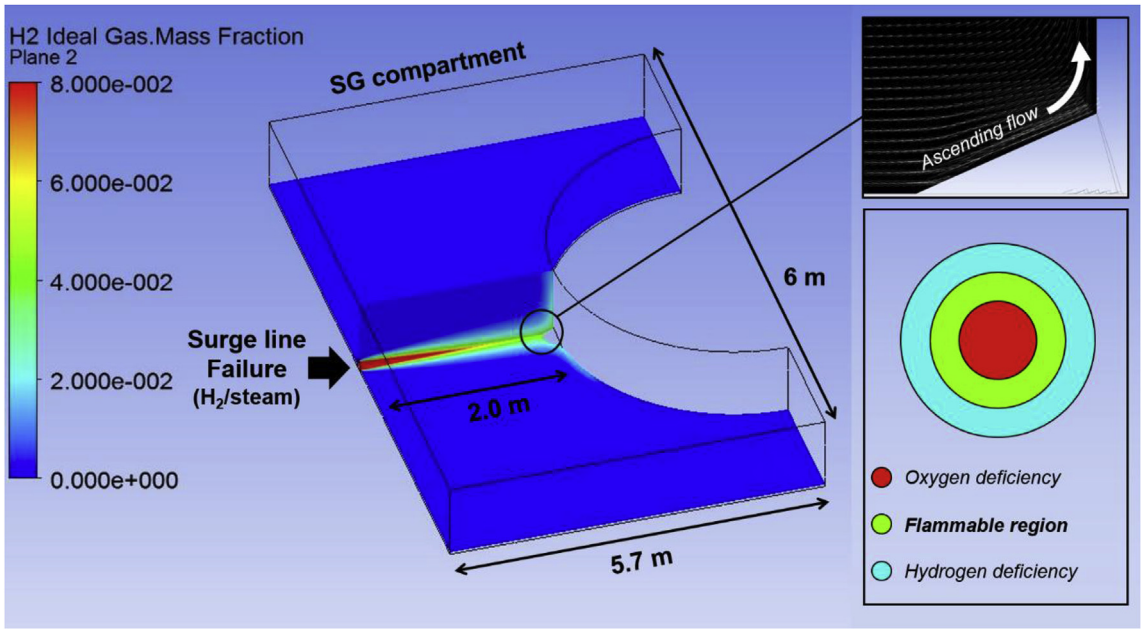

Fig. 11. CFX global contour of the SG compartment after 10 ms.

than jet flow. However, Fig. 13 identified that the data points at the vicinity between flow and atmosphere were still in the flammable region. Consequently, probabilistic ignition can cause the combustion of the gas mixture in the dome by continuous flame propagation of the rising gases.

Further, no flammability was observed using the MELCOR code for the gas mixtures in the SG compartment when the surge line rupture occurred. On the contrary, the CFX code results predicted that the flammable area continuously existed at the interface between the jet and ambient even in the rising hydrogen mixtures. As the current CFX simulation is limited in the modeling of the actual plant geometry, the identification of the rising flammable gases does not guarantee the possibility of hydrogen combustion in the dome area. However, this study confirmed that the MELCOR code, which is the representative severe accident analysis code, can underestimate the possibility of combustible gas generation in a gas jet situation. This difference occurs as, unlike in the MELCOR code, the CFX code solves the 3D fluid dynamic transport with the set of equations including the continuity, momentum, and energy equations for the analysis of the gas behavior.

5. Conclusion

In this study, predictions of hydrogen flammability during a severe accident were compared using the MELCOR and CFX codes. The accident scenario was based on the surge line failure induced by the postulated OPR1000-SBO accident. After the RCS coolant was dried out, the temperature started to rapidly increase. Eventually the surge line failure was predicted at 3.16 h when the averaged wall temperature reached 1200 K, which is similar to the Vierow's MELCOR results. The flammability of the hydrogen gas released upon the failure was analyzed by each of the codes. In conclusion,

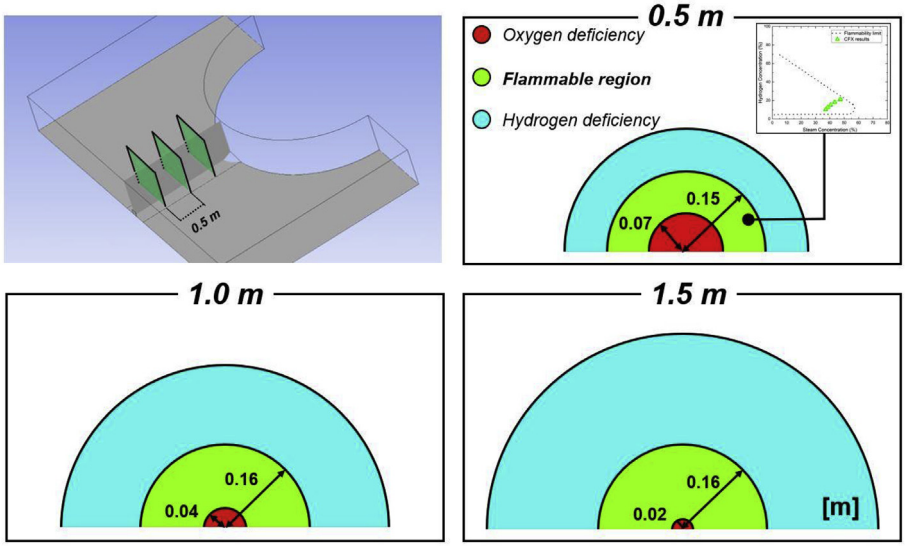

Fig. 12. Flammable region according to distance from the rupture position after 10 ms.

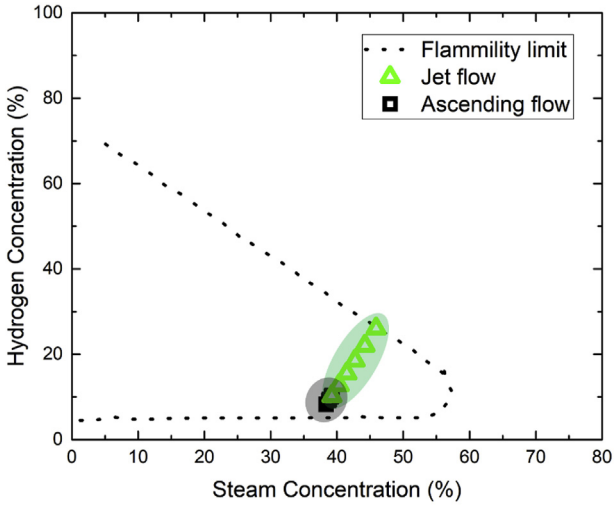

Fig. 13. Presence of the flammable mixtures regardless of the distance from the rupture position.

this study confirmed that the MELCOR code, the representative severe accident analysis code, could underestimate the existence of local combustible gas in turbulent conditions. The major findings of this study can be summarized as follows:

- Until RPV failure, no mixtures with possible flammability were identified by the MELCOR code. Their average hydrogen concentration did not exceed the lower flammability limit measured by Kumar, as the high concentration steam was already present in the compartment at the failure time moment.
- The CFX simulation results showed that local vortices were formed at the beginning of the discharge, leading to a well-developed jet after 10 ms. The discharged gas mixture was dispersed across the compartment at speed over 1000 m/s and hit the SG. After it encountered the SG, the ascending flow was predicted to dominate the overall flow.
- As the released gas mixture was dispersed in the radial direction into the SG compartment, the hydrogen concentration radially decreased, but the oxygen concentration increased. Consequently, both hydrogen and oxygen concentrations outside the formed jet belonged to the combustible region.
- The almost constant flammable area as across the compartment suggests that the jet flow can generate continuous flames by ignition. The existence of flammable mixture was maintained even in the ascending mixture after it encountered the SG. Consequently, probabilistic ignition might cause the combustion of the gas mixture in the dome area by continuous flame propagation of the rising gases.
- As the current CFX simulation is limited in modeling of the actual plant geometry, the identification of the rising flammable gases does not guarantee the occurrence of hydrogen combustion in the dome area. Therefore, more detailed studies on the structural effect should be performed for an accurate hydrogen risk analysis. In addition, vigorous studies of the turbulent effects on flammability limit are still required for nuclear safety.

Declarations of interest

None.

Acknowledgements

This work was supported by the National Research Foundation of Korea (NRF) funded by the Ministry of Science & ICT (MSIT, Korea) [Grant no. NRF-2017M2A8A4018213] and the Nuclear Safety Research Program through the Korea Foundation of Nuclear Safety (KoFONS) using the financial resource granted by the Nuclear Safety and Security Commission (NSSC) of the Republic of Korea (no. 1805001).

Appendix A. Supplementary data

Supplementary data to this article can be found online at https://doi.org/10.1016/j.net.2019.06.024.

References

[1] T. Nishimura, H. Hoshi, A. Hotta, Current research and development activities on fission products and hydrogen risk after the accident at Fukushima Daiichi Nuclear Power Station, Nucl. Eng. Technol. 47 (2015) 1–10.

[2] A. Bentaib, N. Meynet, A. Bleyer, Overview on hydrogen risk research and development activities: methodology and open issues, Nucl. Eng. Technol. 47 (2015) 26–32.
[3] K. Vierow, Y. Liao, J. Johnson, M. Kenton, R. Gauntt, Severe accident analysis of a PWR station blackout with the MELCOR, MAAP4 and SCDAP/RELAP5 codes, Nucl. Eng. Des. 234 (2004) 129–145.
[4] R.O. Gauntt, et al., MELCOR Computer Code Manuals Version 1.8.6, Sandia Natl. Lab., 2005. SAND 2005–5713.
[5] B.E. Boyack, et al., MELCOR Peer Review, Los Alamos Natl. Lab., 1992. LA-12240.
[6] N.K. Kim, J. Jeon, W. Choi, S.J. Kim, Systematic hydrogen risk analysis of OPR1000 containment before RPV failure under station blackout scenario, Ann. Nucl. Energy 116 (2018) 429–438.
[7] W. Choi, S.O. Yu, S.J. Kim, Efficacy analysis of hydrogen mitigation measures of CANDU containment under LOCA scenario, Ann. Nucl. Energy 118 (2018) 122–130.
[8] H.C. Kim, N.D. Suh, J.H. Park, Hydrogen behavior in the IRWST of APR1400 following a station blackout, Nucl. Eng. Technol. 38 (2006) 195–200.
[9] J. Wang, Y. Zhang, K. Mao, Y. Huang, W. Tian, et al., MELCOR simulation of core thermal response during a station blackout initiated severe accident in China pressurized reactor (CPR1000), Prog. Nucl. Energy 81 (2015) 6–15.
[10] J.M. Martín-Valdepeñas, M.A. Jimenez, F. Martin-Fuertes, J.A. Fernandez, Improvements in a CFD code for analysis of hydrogen behaviour within containments, Nucl. Eng. Des. 237 (2007) 627–647.
[11] C. Spengler, S. Arndt, S. Beck, J. Eckel, et al., Further Development of the Computer Codes COCOSYS and ASTEC, Gesellschaft fuer Anlagen- und Reaktorsicherheit mbH, GRS, 2014. GRS-358.
[12] RELAP4/MOD5, A Computer Program for Transient Thermal-Hydraulic Analysis of Nuclear Reactors and Related Systems User's Manual, vol. 1, Idaho Nucl. Eng. Lab., 1976. ANCR-NUREG-1335.
[13] CCPS, Understanding Atmospheric Dispersion of Accidental Releases, AIChE, New York, 1995, 6–8 and 35.
[14] S. Sklavounos, F. Rigas, Validation of turbulence models in heavy gas dispersion over obstacles, J. Hazard Mater. 108 (2004) 9–20.
[15] ANSYS Academic Research, ANSYS CFX User Guide, Release 17.0, ANSYS, Inc, 2015.
[16] Korea Hydro, Nuclear Power Co, Shin Kori 1&2 Final Safety Analysis Report, Seoul, Korea, 2008.
[17] J. Jeon, W. Choi, N.K. Kim, S.J. Kim, Numerical investigation of in-vessel core coolability of PWR through an effective safety injection flow model using MELCOR simulation, Ann. Nucl. Energy 121 (2018) 350–360.
[18] J. Kim, S.W. Hong, S.B. Kim, H.D. Kim, 3-Dimensional analysis of the steam-hydrogen behavior from a small break loss of coolant accident in the APR1400 containment, Nucl. Eng. Technol. 36 (2004) 24–35.
[19] A.M. Gomez-Torres, E. Sainz-Mejia, J.V. Xolocostli-Munguia, et al., CFD analysis of hydrogen volumetric concentrations in a hard venting containment system of MARK-2 BWR, Ann. Nucl. Energy 85 (2015) 552–565.
[20] T. Szabó, F. Kretzschmar, T. Schulenberg, Obtaining a more realistic hydrogen distribution in the containment by coupling MELCOR with GASFLOW, Nucl. Eng. Des. 269 (2014) 330–339.
[21] American National Standards Institute, Design Basis for Protection of Light Water Nuclear Power Plant against the Effects of Postulated Pipe Rupture, 1988. ANSI/ANS-58.2-1988.
[22] R.K. Kumar, Flammability limits of hydrogen–oxygen–diluent mixtures, J. Fire Sci. 3 (1985) 245–262.
[23] J. Jeon, W. Choi, S.J. Kim, A flammability limit model for hydrogen-air-diluent mixtures based on heat transfer characteristics in flame propagation, Nucl. Eng. Technol., https://doi.org/10.1016/j.net.2019.05.005
[24] T. Aldemir, A survey of dynamic methodologies for probabilistic safety assessment of nuclear power plants, Ann. Nucl. Energy 52 (2013) 113–124.
[25] M. Heitsch, R. Huhtanen, Z. Téchy, et al., CFD evaluation of hydrogen risk mitigation measures in a VVER-440/213 containment, Nucl. Eng. Des. 240 (2010) 385–396.
[26] B.W. Marshall, Hydrogen:Air:Steam Flammability Limits and Combustion Characteristics in the FITS Vessel, Report No. SAND84-0383, Sandia National Lab., 1986.
[27] J. Kim, S.W. Hong, Analysis of hydrogen flame acceleration in APR1400 containment by coupling hydrogen distribution and combustion analysis codes, Prog. Nucl. Energy 78 (2015) 101–109.